An Improved Sequential-Model Predictive Control for an O-Z-Source Inverter Without Weighting Factors

Xuan WANG and Wei LUO

***Abstract*—When finite set model predictive control is applied to an O-Z-source inverter (O-ZSI) containing a transformer, there are multiple control variables, it is difficult to adjust the weighting factors, and the currents on both sides of the transformer could change abruptly, making it impossible to calculate and derive reference values to directly predict and control the currents on both sides of the transformer. In this paper, an improved sequential-model predictive control is proposed for O-ZSI with a transformer without adjusting the weighting factors. By equating the transformer as a parallel connection of the excitation inductance with a set of ideal transformers without adjusting the weighting factors, the reference value of the magnetization current of the excitation inductance can be calculated according to the theoretical derivation, which can realize the predictive control of the O-ZSI. Simulation analysis and experimental results show that the proposed control method achieves the sequential-model predictive control of O-ZSI without adjusting the weight factors, with good steady-state and dynamic characteristics.**

***Index Terms*—O-Z-source inverter, sequential-model prediction, transformer, weighting factors.**

I. Introduction

THE Z-source inverter (ZSI) could achieve a boost function by the shoot-through state, however the ZSI has a large start-up inrush current, and in the impedance network, the stress on the capacitor voltage and the inductor current is significant [1], [2]. The quasi-Z-source inverter (q-ZSI) is an improvement of the ZSI. Not only does it inherit the advantages of the ZSI, but it also has the benefits of reduced stress on the capacitor voltage and inductor current, as well as continuous input current. However, the output voltage gain has not been increased [3]. [4], [5] proposed transformer-based Z-source networks, Trans-Z-source converters and Γ-Z-source converters, effectively enhance power density, reduce system costs, and improve the system's boosting capability through the precise control of the transformer's turns ratio.

However, they still have the problem of discontinuous power input current and starting inrush current [6], [7]. Without increasing the system cost, the O-Z source inverter based on O-type impedance network applied in this paper can reduce the capacitor voltage stress and effectively suppress the start-up inrush current. The O-Z source topology is similar to the Trans-Z source and Γ-Z source, both of which can be classified as a transformer-based Z source topology. Compared to existing Z-source topologies, the boosting capacity can be improved by adjusting the transformer turn ratio, effectively solving the excessive stress on the capacitor, and suppressing the start-up inrush current with fewer required components and a compact structure [8]–[10]. Based on the above advantages, the O-ZSI can be applied to the grid-connected renewable energy generation systems [11].

In recent years, with the rapid development of digital signal processing technology, finite-control-set MPC (FCS-MPC) has many advantages such as a simple control principle, easy digital implementation and fast dynamic response [12]–[14]. Many scholars have applied FCS-MPC to the control of Z-source topology and achieved good performances [15]–[17]. However, FCS-MPC in the above literature is applied to Z-source topologies without transformers (ZSI or q-ZSI, etc.). For Z-source topologies containing transformers (trans-ZSI, Γ-ZSI or O-ZSI), the currents on both sides of the transformer will abruptly change [18]. Unlike the reference value of the inductor current can be calculated according to theoretical derivation in the inductor current ZSI or q-ZSI [19]–[21], so it is not possible to directly predict and control the current on both sides of the transformer. In this paper, the O-ZSI is equivalent to the parallel connection of a set of ideal transformers of magnetizing inductance with a set of ideal transformers. The reference value of the magnetization current i_m of the magnetizing inductance is derived according to the theory, and the transformer is controlled by controlling the magnetization current. Then, the FCS-MPC of O-ZSI with transformer is realized.

In the O-ZSI control system, the cost function constructed by the conventional FCS-MPC usually includes three control objects: inductor current, capacitor voltage, and output current [22]–[24], each of which should have a weighting factor to reflect the importance of the control quantity [25]–[27]. However, weighting factors are often selected based on experiences and lack theoretical guidance [27]. Many scholars have examined how to eliminate the weighting factors. In the field of electric machines, [28] calculated the optimal weighting factors of stator flux linkage online based on the principle of minimum torque ripple. However, the mathematical expression of the optimal weighting factors is complex and

Manuscript received May 30, 2023; revised November 30, 2023 and January 2, 2024; accepted January 29, 2024. Date of publication June 30, 2024; date of current version February 7, 2024. No funding was received to assist with the preparation of this manuscript. *(Corresponding author: Wei Luo.)*

Both authors are with the Department of Electrical Engineering, University of Shanghai for Science and Technology, Shanghai, China (e-mail: 1195403809@qq.com; luowei@usst.edu.cn).

Digital Object Identifier 10.24295/CPSSTPEA.2024.00002

depends on accurate motor parameters. In [29], an algebraic weighting factor selection method was proposed to achieve similar performance for predictive current control. Although the calculation of the weighting factors is simpler than that in [28], it still depends on the electrical parameters and system state. In [30], a multi-objective optimization method based on ranking is proposed. The cost function value of the torque and stator flux linkage in each switching state is transformed into a ranking value; then, the switching state with the smallest average ranking value is selected as the optimal switching state. Although this method avoids to design weighting factors, it increases the computational burden and control complexity. In [31], Professor Rodriguez proposed a sequential-model predictive control (S-MPC) strategy applied to the control of a motor by first selecting the two smallest switching states using the cost of torque and subsequently selecting the least costly switching state from two alternative switching states using the cost function of the magnetic flux, which eliminated the weighting factors of the traditional MPC in motor control field. However, this method has not been extended to the inverter with a transformer, and removing many switching states at one time may lead to inaccurate results. [32] analyzes the current by transforming it into the $\alpha\beta$ coordinate system, which introduces an additional control object and increases a cost function. This approach improves the accuracy of the results. [33], [34] apply this approach though improves the cost function and eliminates weighting factors by using the S-MPC method. However, the excessive elimination of voltage vectors each time may led to a reduction in prediction accuracy.

This paper applies a sequential-model predictive control to O-ZSI and proposes a sequential-MPC without weighting factors for O-ZSI. First, the O-ZSI topology is analyzed, its discrete mathematical model is established, and the prediction functions of the inductor current, capacitance voltage, and output current are derived. Then, the steady-state model of the O-ZSI is analyzed, the reference values of each control variable are derived, and the sequential-MPC method applied to the O-ZSI is proposed. Finally, the simulation analysis based on MATLAB/Simulink is performed, and an experimental prototype is built to verify the correctness and effectiveness of the proposed strategy in the O-ZSI with a transformer.

II. O-ZSI Model and Analysis

A. Discrete Mathematical Model for O-ZSI

The topology of the O-ZSI is shown in Fig. 1 and consists of the power supply v_{in}, an O-Z source network, a three-phase inverter bridge, and a three-phase resistive inductive load. The O-Z source network consists of diode D, capacitor C and a double-winding transformer, which is composed of the dotted terminals of the double-winding transformer, with the primary and secondary winding turn ratio γ.

$$\gamma = N_1 / N_2 \tag{1}$$

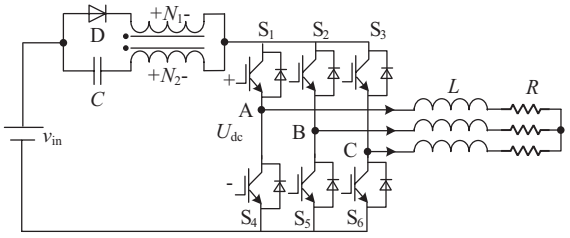

Fig. 1. O-ZSI topology.

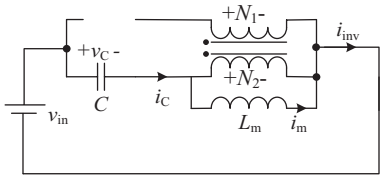

(a) Shoot-through state

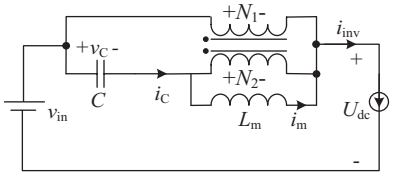

(b) Non-shoot-through state

Fig. 2. Equivalent circuits of O-ZSI.

where N_1 is the number of turns of the primary winding of the double-winding transformer, and N_2 is the number of turns of the secondary winding of the double-winding transformer.

The O-ZSI and ZSI have similar basic principles and can be divided into two operating cases: the shoot-through state and the non-shoot-through state. The equivalent circuit for the two operating cases of O-ZSI is shown in Fig. 2. In the diagram, the transformer is equivalent to the parallel connection of the magnetizing inductance L_m and a set of ideal transformers.

Considering all possible switching states of the six switches, Table I lists the output voltage vectors of the inverter for the simplified eight switching states.

The output voltage vector can be expressed as follows:

$$V_x = \frac{2U_{dc}}{3}(S_A + aS_B + a^2 S_C) \tag{2}$$

where the unit vector $a = e^{j2\pi/3}$ represents the 120° phase difference between phases, $x = [0,7]$. U_{dc} is the DC-link voltage of the inverter after boosting by the O-Z network. S_A, S_B, and S_C are the switching states of the three-phase upper arms of inverter bridges A, B, and C, respectively.

The current dynamic equation of the load current in the stationary $\alpha\beta$ coordinate system is:

$$\begin{cases} L\dfrac{di_\alpha}{dt} = V_\alpha - Ri_\alpha \\ L\dfrac{di_\beta}{dt} = V_\beta - Ri_\beta \end{cases} \tag{3}$$

TABLE I
OUTPUT VOLTAGE OF THE O-ZSI FOR DIFFERENT SWITCHING CASES

State	v_o	S_1	S_2	S_3	S_4	S_5	S_6
Non-shoot-through state	V_0	0	0	0	1	1	1
	V_1	1	0	0	0	1	1
	V_2	1	1	0	0	0	1
	V_3	0	1	0	1	0	1
	V_4	0	1	1	1	0	0
	V_5	0	0	1	1	1	0
	V_6	1	0	1	0	1	0
Shoot-through state	V_7	1	1	1	1	1	1

where i_α and i_β are the α and β components of the inverter output current vector in the $\alpha\beta$ coordinate system. V_α and V_β are the α and β components of the inverter output voltage vector in the $\alpha\beta$ coordinate system. The sampling period of the system is set to T_s. The derivative of the output current in these equations is equated using the forward Euler equations as:

$$\begin{cases} \dfrac{\mathrm{d}i_\alpha}{\mathrm{d}t} = \dfrac{i_\alpha(k+1) - i_\alpha(k)}{T_s} \\ \dfrac{\mathrm{d}i_\beta}{\mathrm{d}t} = \dfrac{i_\beta(k+1) - i_\beta(k)}{T_s} \end{cases} \tag{4}$$

Substitute (4) into (3) and simplify to obtain:

$$\begin{cases} i_\alpha(k+1) = \dfrac{T_s}{L} V_\alpha(k) + \left(1 - \dfrac{RT_s}{L}\right) i_\alpha(k) \\ i_\beta(k+1) = \dfrac{T_s}{L} V_\beta(k) + \left(1 - \dfrac{RT_s}{L}\right) i_\beta(k) \end{cases} \tag{5}$$

where $i_\alpha(k)$ and $i_\beta(k)$ are the current components in the $\alpha\beta$ coordinate system at t_k (sampling time k); $i_\alpha(k+1)$ and $i_\beta(k+1)$ are the predicted values of the current component in the $\alpha\beta$ coordinate system at t_{k+1}; $V_\alpha(k)$ and $V_\beta(k)$ are the voltage components in the $\alpha\beta$ coordinate system at t_k sampling times.

When the O-ZSI is in both shoot-through state and non-shoot-through state, we derive the equations for the magnetization current and capacitance voltage flowing through the transformer excitation inductor L_m as follows:

1) *Shoot-Through States*

According to the equivalent circuit in Fig. 2(a), the following circuit equations can be written:

$$\begin{cases} L_m \dfrac{\mathrm{d}i_m}{\mathrm{d}t} = v_{in} - v_C \\ C \dfrac{\mathrm{d}v_C}{\mathrm{d}t} = i_m \end{cases} \tag{6}$$

where i_m is the magnetization current of the magnetizing inductance L_m, and the derivative of the magnetization current i_m and capacitance voltage v_C is approximated by the forward Euler:

$$\begin{cases} \dfrac{\mathrm{d}i_m}{\mathrm{d}t} = \dfrac{i_m(k+1) - i_m(k)}{T_s} \\ \dfrac{\mathrm{d}v_C}{\mathrm{d}t} = \dfrac{v_C(k+1) - v_C(k)}{T_s} \end{cases} \tag{7}$$

Substituting (7) into (6) and simplifying it yield:

$$\begin{cases} i_m(k+1) = \dfrac{T_s}{L_m}\left[v_{in} - v_C(k)\right] + i_m(k) \\ v_C(k+1) = \dfrac{T_s}{C} i_m(k) + v_C(k) \end{cases} \tag{8}$$

where $i_m(k)$ and $v_C(k)$ are the sampling values of the magnetization current i_m and capacitance voltage v_C of the transformer magnetizing inductance L_m at t_k and in the shoot-through state, respectively. $i_m(k+1)$ and $v_C(k+1)$ are the predicted values of magnetization current i_m and capacitance voltage v_C of the transformer magnetizing inductance L_m at $k+1$ and in the shoot-through state, respectively.

2) *Non-Shoot-Through State*

According to the equivalent circuit in Fig. 2(b), the following circuit equations can be listed:

$$\begin{cases} (\gamma - 1) L_m \dfrac{\mathrm{d}i_m}{\mathrm{d}t} = v_C \\ (\gamma - 1) C \dfrac{\mathrm{d}v_C}{\mathrm{d}t} = \gamma i_{inv} - i_m \end{cases} \tag{9}$$

where i_{inv} is the output current of the O-Z source network. At t_k, $i_{inv}(k) = i_A(k)S_A + i_B(k)S_B + i_C(k)S_C$ can be calculated by sampling the three-phase current at the load side and switching states S_A, S_B, and S_C.

When the ratio of turns is $\gamma = 2$, substitute (7) into (9) and simplify it to obtain:

$$\begin{cases} i_m(k+1) = \dfrac{T_s}{L_m} v_C(k) + i_m(k) \\ v_C(k+1) = \dfrac{2i_{inv}(k) - i_m(k)}{C} T_s + v_C(k) \end{cases} \tag{10}$$

where $i_m(k)$ and $v_C(k)$ are the sampled values of the magnetization current i_m and capacitance voltage v_C of the transformer magnetizing inductance L_m at t_k and in the non-shoot-through state, respectively. $i_m(k+1)$ and $v_C(k+1)$ are the predicted values of the magnetization current i_m and capacitor voltage v_C of the transformer excitation inductor L_m at t_{k+1} and in the non-shoot-through state, respectively.

B. O-ZSI Prediction Function

In the analysis of the O-ZSI discrete model, the transformer is equivalent to the parallel connection of the excitation inductance L_m with a set of ideal transformers. i_m is the current flowing through the excitation inductance, which cannot be directly measured but can be expressed by $i_{inv}(k)$ and $i_C(k)$.

In the shoot-through state, the N_1 side is disconnected because diode D withstands a reverse pressure in the reverse cutoff state, and obtain:

$$i_m = i_C = i_{inv} \tag{11}$$

Therefore, in the shoot-through state, the predicted values of the transformer excitation inductance current i_m and capacitor voltage v_C, $i_m(k+1)$ and $v_C(k+1)$, can be rewritten in combination with (8) and (11) as follows:

$$\begin{cases} i_m(k+1) = \dfrac{T_s}{L_m}\left[v_{inv} - v_C(k)\right] + i_{inv}(k) \\ v_C(k+1) = \dfrac{T_s}{C} i_{inv}(k) + v_C(k) \end{cases} \tag{12}$$

In a non-shoot-through state, it can be concluded that:

$$\begin{cases} i_{N_1} = -i_{N_2}/2 \\ i_{N_2} = i_C - i_m \\ i_{N_1} + i_{N_2} + i_m = i_{inv} \end{cases} \tag{13}$$

The above equations can be combined to obtain:

$$i_m = 2i_{inv} - i_C \tag{14}$$

In the non-shoot-through state, the predicted values $i_m(k+1)$ and $v_C(k+1)$ can be rewritten by combining (10) and (14):

$$\begin{cases} i_m(k+1) = \dfrac{T_s}{L_m} v_C(k) + 2i_{inv}(k) - i_C(k) \\ v_C(k+1) = \dfrac{i_C(k)}{C} T_s + v_C(k) \end{cases} \tag{15}$$

C. O-ZSI Steady-State Model

According to the three-phase symmetrical load parameters in Fig. 1:

$$i_{om} = \sqrt{\frac{2P_o}{3R}} \tag{16}$$

where i_{om} and P_o are the output phase current peak and power, respectively.

The control period is T_s, the shoot-through time is T_0, and the shoot-through duty cycle is $D_0 = T_0/T_s$. Using the state-space averaging method, the steady-state capacitance voltage v_C and magnetizing inductance current i_m that flows through the transformer can be expressed as:

$$\begin{cases} V_C = \dfrac{D_0(\gamma - 1)}{\gamma D_0 - 1} v_{in} \\ I_m = \dfrac{(1 - D_0)\gamma}{1 - \gamma D_0} i_{inv} \end{cases} \tag{17}$$

From (17), the DC-link voltage U_{dc} of the inverter in the non-shoot-through state can be obtained:

$$U_{dc} = v_{in} - v_{N_1} = v_{in} - \frac{\gamma}{\gamma - 1} V_C = \frac{1}{1 - \gamma D_0} v_{in} = B v_{in} \tag{18}$$

where B is the boost factor, and $B = 1/(1-D_0)$.

According to the conservation of energy, the average input current on the power side can be obtained:

$$i_{in} = \frac{1 - D_0}{1 - \gamma D_0} i_{inv} = \frac{P_o}{v_{in}} \tag{19}$$

Substituting (19) into (17), obtain the relationship between the magnetized inductor current and the average input current on the power supply side at steady state:

$$I_m = \gamma i_{in} \tag{20}$$

III. O-ZSI Improved Sequential-Model Predictive Control

In this paper, taking the O-ZSI with a transformer as an example, the model predictive control with transformer is solved, and a sequential-model predictive control is designed to eliminate the weighting factors. To solve the model equated as a parallel connection of the magnetizing inductance L_m with a set of ideal transformers. The magnetization current i_m of the magnetizing inductance is continuous, so the magnetization current i_m of the magnetizing inductance can be controlled to control the transformer. The magnetization current i_m can be converted predictive control of transformer O-ZSI, the transformer is according to (11) and (15).

A. Traditional FCS-MPC Control Strategy

In the traditional FCS-MPC strategy, the cost function of O-ZSI requires at least three weight factors can be expressed:

$$\begin{aligned} g = {} & \lambda_L [I_{m\_ref}(k) - i_m(k+1)]^2 + \lambda_C \left[V_{C\_ref}(k) - v_C(k+1)\right]^2 + \\ & \lambda_i [I_{\alpha\_ref}(k) - i_\alpha(k+1)]^2 + \lambda_i \left[I_{\beta\_ref}(k) - i_\beta(k+1)\right]^2 \end{aligned} \tag{21}$$

where $I_{m\_ref}(k)$ and $V_{C\_ref}(k)$ is the inductive current and capacitive voltage reference, respectively. $i_{\alpha\_ref}(k)$ and $i_{\beta\_ref}(k)$ are the $\alpha\beta$-axis components of the reference output current, $i_\alpha(k+1)$ and $i_\beta(k+1)$ are the $\alpha\beta$-axis components of the output current

prediction; λ_L, λ_C and λ_i are the weighting factors for inductor current, capacitor voltage and output current, respectively.

For a three-phase symmetrical load, the corresponding reference value of the control object can be obtained:

$$\begin{cases} i_{\text{inv\_ref}} = \sqrt{\dfrac{2P_o}{3R}} \\ V_{\text{C\_ref}} = \dfrac{D_0(\gamma-1)}{\gamma D_0 - 1} v_{\text{in}} \\ I_{\text{m\_ref}} = \dfrac{(1-D_0)\gamma}{1-\gamma D_0} i_{\text{inv}} \end{cases} \tag{22}$$

B. The Proposed S-MPC Strategy Without Weighting Factors

It is generally recognized that there is no relevant relationship between the capacitor voltage and the load current, therefore the weighting factor is inevitably required to weigh the two variables. But the tuning of the weighting factors is usually a complex process. The following is the method of eliminating the weighting factors proposed in this paper for the model prediction of O-ZSI.

The cost function in this article is the error between reference value and predicted value:

$$\begin{cases} g_m = \left| I_{\text{m\_ref}} - i_m(k+1) \right| \\ g_C = \left| V_{\text{C\_ref}} - v_C(k+1) \right| \\ g_\alpha = \left| i_{\alpha\_\text{ref}} - i_\alpha(k+1) \right| \\ g_\beta = \left| i_{\beta\_\text{ref}} - i_\beta(k+1) \right| \end{cases} \tag{23}$$

where $i_{\text{m\_ref}}$ is the reference value of the magnetization current of the transformer magnetizing inductance L_m at steady state; $v_{\text{C\_ref}}$ is the reference value of the capacitor voltage at steady state; i_{α_ref} and i_{β_ref} is the α and β components of the output current reference values in the $\alpha\beta$ coordinate system.

In the traditional sequential-model predictive control (S-MPC1), first, determine n control objects. These objects are then sorted according to their priority, with each control object defining a separate cost function. In the cost function g_1, l available switch states are calculated, and the n switch states that minimize the cost function g_1 are selected for regulating the first control object.

In the cost function g_2, all n available switch states are calculated, and the $n-1$ switch states that minimize the cost function g_2 are selected for regulating the second control object.

In the cost function g_{x-1}, all n-x+3 available switch states are calculated, and the $n-x$+2 switch states that minimize the cost function g_{x-1} are selected for regulating the $x-1$ control object.

In this paper, capacitor voltage and the $\alpha\beta$-axis current component of the output current, which are selected as control objects, switching states equal to 2^3 available switching states are calculated, and n is the control objects equals to three, removing one of the shoot-through state variables, so l equals to seven. Therefore, seven available switch states are calculated, and the three switch states that minimize the cost function g_c are selected for the next cycle. In the cost function g_α, three available switch states are calculated, and the two switch states that minimize g_α are selected. This process is repeated in g_β, where two available switch states are calculated, and the switch state that minimizes g_β is selected.

The proposed sequential-model predictive control (S-MPC2) can be realized by the following steps, first identify n control objects and m switching states, each control object defines a separate cost function that is computed sequentially.

In this paper, n is the control objects also equals to three, removing one of the shoot-through state variables, so m equals to seven. In order not to increase the computational burden and to have enough voltage vectors to be analyzed, a fixed-step formula was proposed and the optimal result is equals to two that obtained by screening the step size:

$$S = (m-1)/n \tag{24}$$

Therefore, seven available switch states are calculated, and the five switch states that minimize the cost function g_c are selected for the next cycle. In the cost function g_α, five available switch states are calculated, and the three switch states that minimize g_α are selected. This process is repeated in g_β, where three available switch states are calculated, and the switch state that minimizes g_β is selected.

Based on the mathematical model of O-ZSI and advantages of S-MPC, this paper designs the O-ZSI sequential-model predictive control. The algorithm execution flowchart is shown in Fig. 3. The magnetization current i_m of the excitation inductor decreases when the O-ZSI is in the non-shoot-through state and increases when it is in the shoot-through state. Based on this characteristic, this paper determines whether the next control cycle is in the shoot-through state according to the predicted magnetization current i_m. First, using the cost function g_m in (23), we determine whether the next switching state of the inverter is in the shoot-through state based on the predicted $i_m(k+1)$ of the magnetization current i_m of the transformer magnetizing inductance L_m in the shoot-through state and non-shoot-through state.

In the shoot-through state, all switches of the inverter bridge are turned on. In seven non-shoot-through states, first, the predictive capacitor voltage is first calculated using (15); then, the cost function g_C of the capacitor voltage in (23) is calculated. The two switching states that make the capacitor voltage most costly are eliminated from the seven non-shoot-through states. The remaining five non-shoot-through switching states are temporarily selected. Using (5), the predicted output current in the remaining five non-shoot-through states is calculated. Then, the cost function g_α of the load current in (23) is calculated, eliminating the two switching states that make the load current α-axis component the costliest. Among the remaining three switching states, the β-axis component cost function is calculated using (23), and the two switching states that maximize the cost are eliminated, and the remaining optimal non-shoot-through switching state is selected. Finally, the remaining optimal non-shoot-through switching state is selected and applied

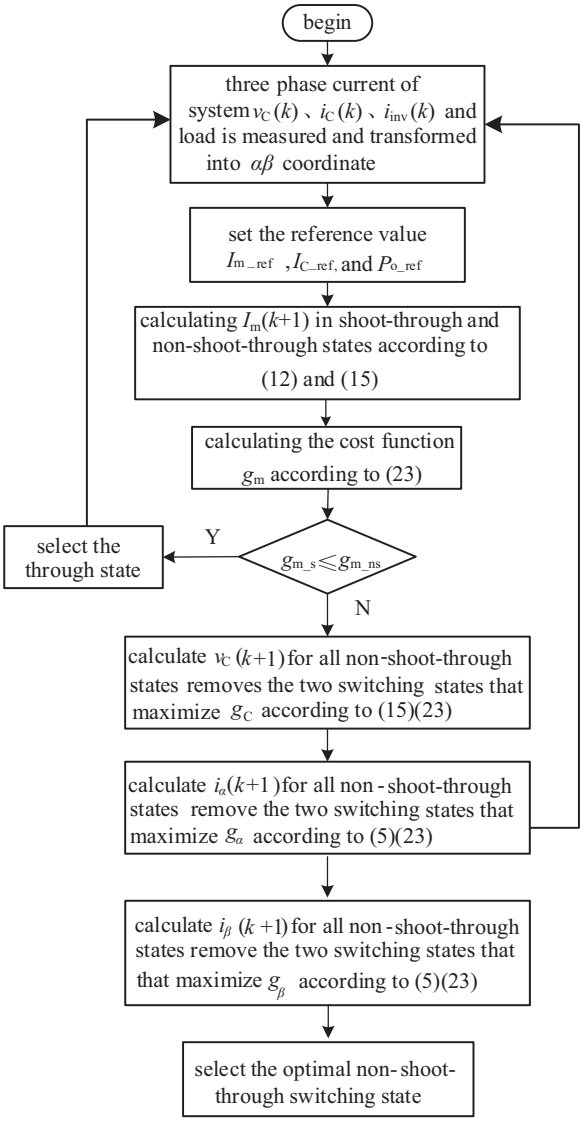

Fig. 3. Model predictive control execution flow chart for O-ZSI.

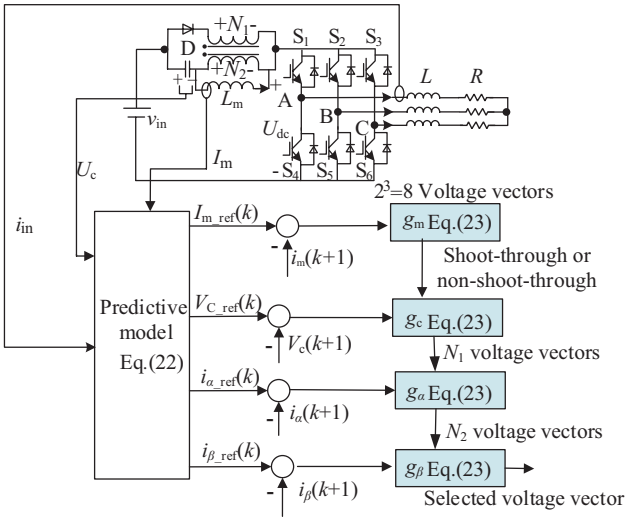

Fig. 4. Improved sequential-model predictive control block diagram for O-ZSI.

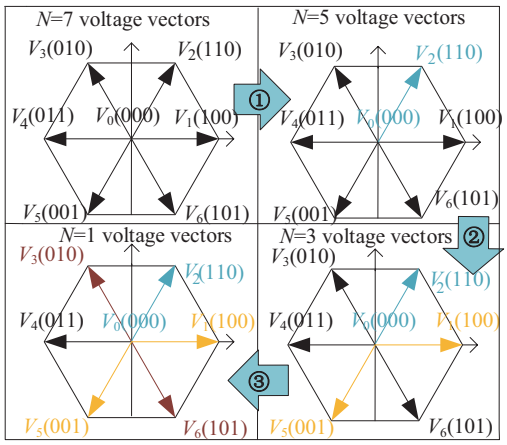

Fig. 5. Example of the voltage vectors used in each step of S-MPC2.

to the next control cycle of O-ZSI.

The above calculations show that the seven switching states have different effects on control effects on the control quantity, and the two switching states with the largest error compared to the expected value are removed by sorting them from the most effective to the least effective, and since n equals to three, the above steps are carried out three times, and the cost functions for the capacitor voltage cost function and the load current $\alpha\beta$ are computed in turn, retaining the rest of the switching states that have a small difference from the expected value.

Since the proposed strategy removes the switching states that make the current cost function the largest, the particularly unsuitable switches have been removed, and the switching states are used as one of the two switching states that can be optionally removed in the conventional cost function, the proposed strategy can effectively reduce the computation burden. The control block diagram of S-MPC algorithm for O-ZSI is shown in Fig. 4.

Fig. 5 is depicted as an example of the voltage vectors used in each step. The first step 1 is removing the two states with the maximum g_c values. The next step 2 is removing the two states with the maximum g_α values. The last step 3 is removing the two states with the maximum g_β values.

IV. Simulation Analysis

To verify the feasibility and effectiveness of the proposed sequential-MPC strategy (S-MPC2) for O-ZSI in this paper, the simulation analysis is performed using MATLAB/Simulink and compared with the traditional FCS-MPC and traditional S-MPC strategy (S-MPC1). The simulation parameters are shown in table II, and the weighting factors of the traditional FCS-MPC in the table are obtained by extensive debugging.

A. Steady-State Performance

Considering the O-ZSI stability under different operating conditions, the output current total harmonic distortion (THD), root mean square error (RMSE) of capacitor voltage, and RMSE of output current in *dq*-axis are tested respectively to

TABLE II
SIMULATION PARAMETERS OF THE O-Z-SOURCE INVERTER

Parameter	Value
Input voltage v_{in}/V	100
O-Z source capacitance C/μF	1000
Transformer primary side self-inductance L_1/μH	2000
Transformer secondary side self-Inductance L_2/μH	500
Transformer mutual inductance L_m/μH	999.9
Turn ratio of primary and secondary Winding of transformer γ	2
Filter inductance L_f/mH	10
Load resistance R/Ω	10
Sampling period T_s /μs	20
Output frequency f/Hz	50 / 100
Weighting factors λ_m, λ_C, λ_α, λ_β	30 / 19.5 / 10 / 9.8

evaluate the control performance. By measuring and evaluating these indicators, we can assess the steady-state performance of the different model predictive control strategy for O-ZSI. Fig. 6 compares the control performance of three strategies, FCS-MPC, S-MPC1, and S-MPC2, under different output power conditions.

The performance of S-MPC2 and FCS-MPC in terms of output current THD is found to be comparable. Additionally, the overall trend of THD increases with an increase in the reference power, while exhibiting minimal fluctuation. On the other hand, S-MPC1 shows consistently higher THD values and greater volatility compared to FCS-MPC and S-MPC2.

The RMSE of capacitor voltage shows that S-MPC1 exhibits a relatively larger error, whereas FCS-MPC and S-MPC2 demonstrate similar trends. However, under most conditions, S-MPC2 exhibits slightly better performance than FCS-MPC. Analyzing the RMSE of output current reveals that FCS-MPC is relatively stable compared to S-MPC2, with a smaller fluctuation range for the $I_{d\text{-axis}}$ component. Conversely, S-MPC2 shows less fluctuation for the $I_{q\text{-axis}}$ output current component.

In a word, the simulation results indicate that S-MPC2 strategy can maintain comparable results to FCS-MPC while reducing computational complexity. In contrast, S-MPC1 shows inferior performance despite its lower computational complexity. Both S-MPC strategies exhibit certain advantages in terms of computational complexity, with S-MPC2 outperforming S-MPC1 in overall performance.

B. Power Step-Change

Letting the input voltage of the system v_{in} = 100 V and the DC-link voltage U_{dc} = 200 V. (17) can calculate V_{C_ref} = −50 V, and (18) can calculate the shoot-through duty cycle D_0 = 0.25. When the output power reference value P_{o_ref} abruptly changes from 1000 W to 540 W, the load phase current peak reference value i_{om_ref} changes from 8.165 A to 6 A.

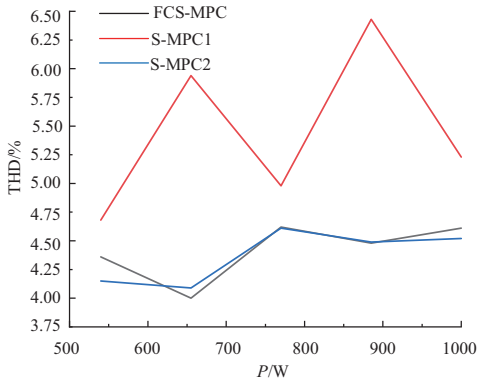

(a) Output current THD of three methods under different output power

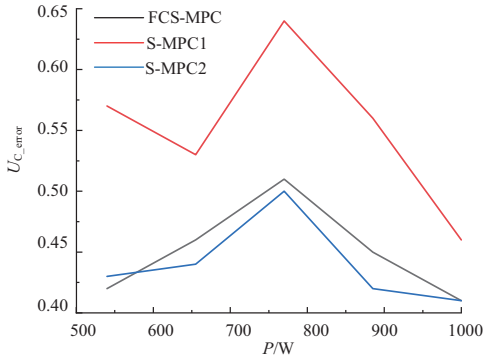

(b) Capacitor voltage RMSE value of three methods under different output power

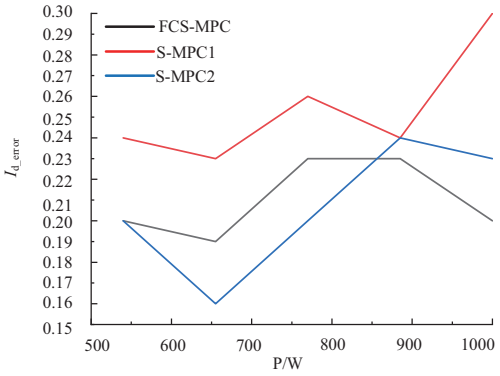

(c) Output current *d*-axis component RMSE value of three methods under different output power

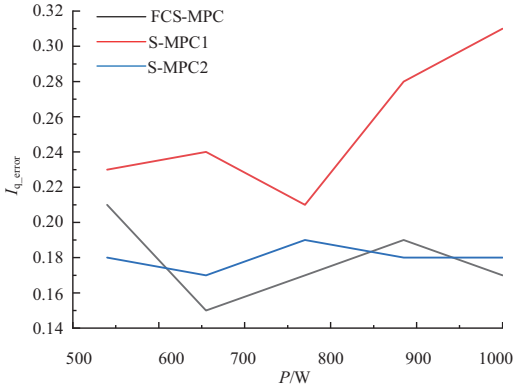

(d) Output current *q*-axis component RMSE value of three methods under different output power

Fig. 6. Steady-state performance of the three strategies under different output power conditions.

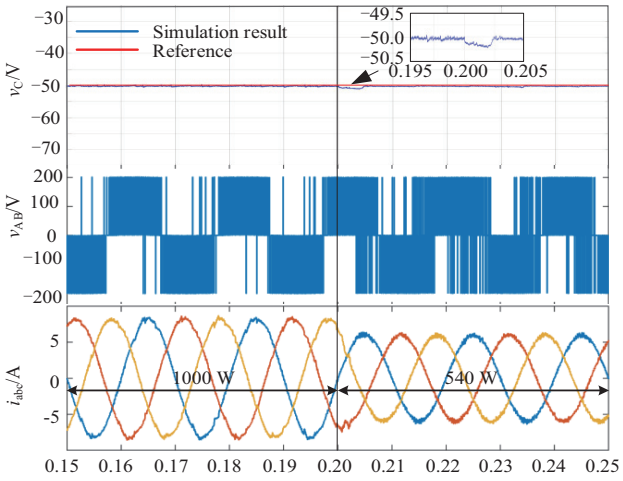

(a) Simulation waveforms in the traditional FCS-MPC strategy

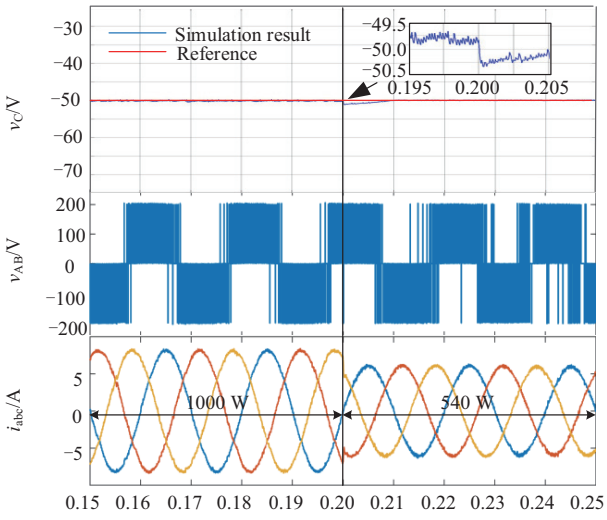

(b) Simulation waveforms in the proposed sequential-MPC strategy

Fig. 7. Output power 1000 W step to 540 W simulation waveform.

Fig. 7(a) is the simulation waveform under the traditional FCS-MPC strategy, and Fig. 7(b) is the simulation waveform of the S-MPC2 proposed in this paper. When the output power step occurs in 0.20 s, the output phase current rapidly follows the reference value under the two strategies, and the peak value changes from 8.165 A to 6 A, while the capacitor voltage basically remains at −50 V. Both strategies achieve model predictive control of O-ZSI and can resist the output power disturbance ability, which can ensure that the system can reliably and stably work when there is this disturbance.

The FFT analysis of the output A-phase current before 0.20 s in Fig. 8 shows that the harmonic distortion rate is 2.96% and 2.68% with the traditional FCS-MPC strategy and S-MPC2 strategy, respectively. The output current waveform quality is better under the proposed sequential-MPC strategy.

C. Frequency Step-Change

Let the input voltage of the system be v_{in} = 100 V, the DC-link voltage be U_{dc} = 200 V unchanged, and the output power reference value be P_{o_ref} = 540 W when the output frequency reference value changes from 50 Hz to 100 Hz.

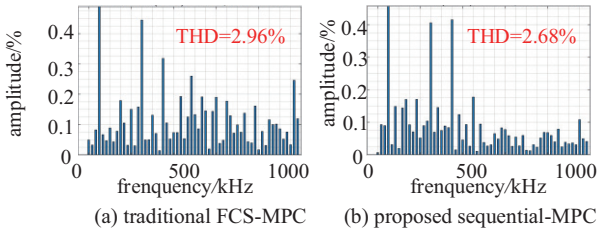

(a) traditional FCS-MPC (b) proposed sequential-MPC

Fig. 8. FFT analysis of the load current under two strategies.

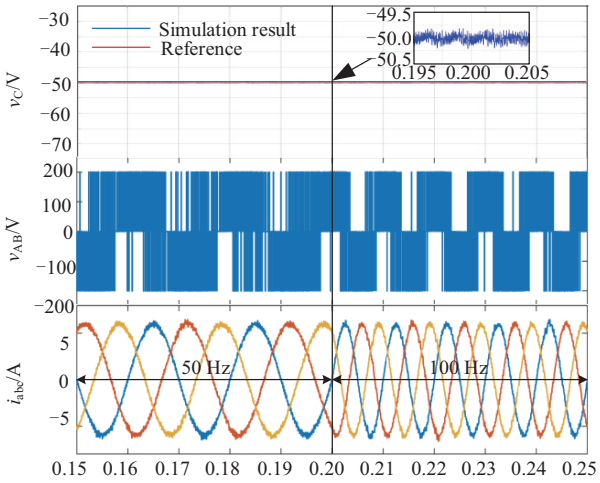

(a) Simulation waveforms in the traditional FCS-MPC strategy

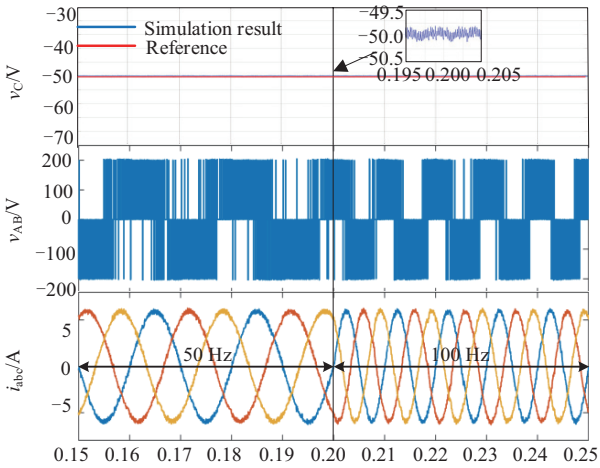

(b) Simulation waveforms in the proposed sequential-MPC strategy

Fig. 9. Output frequency 50 Hz step to 100 Hz simulation waveform.

Fig. 9(a) is the simulation waveform in the traditional FCS-MPC strategy, and Fig. 9(b) is the simulation waveform of the S-MPC2 proposed in this paper. When the output frequency reference value step occurs at 0.20 s, the capacitor voltage remains stable with the two strategies, and the load three-phase current can follow the reference value well, which indicates that both FCS-MPC strategies are resistant to output frequency disturbance.

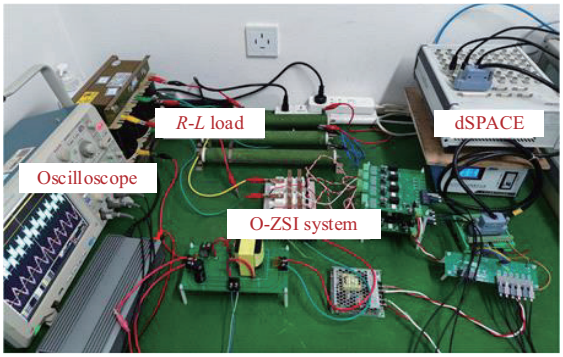

Fig. 10. O-ZSI experimental platform.

V. Experimental Verification

To verify the feasibility of the proposed S-MPC strategy for O-ZSI, an experimental prototype is built, as shown in Fig. 10. The parameters of each component in the main circuit are as follows: the capacitance is C = 1000 μF in the O-Z source topology, the transformer uses a customized high-frequency transformer with low leakage inductance and a 2:1 turn ratio, the IGBT power switch is an FF100R12RT4 from INFINEON, and the filter inductance $L_a = L_b = L_c$ = 10 mH. The control algorithm is implemented based on the dSPACE platform. To avoid electromagnetic interference, the dSPACE output control signal is transmitted to the drive circuit via an optical fiber, which controls the IGBTs.

A. Steady-State Performance

Given the input voltage v_{in} = 100 V and DC-link voltage U_{dc} = 200 V, and the output power reference value P_{o_ref} = 540 W, the experimental results are shown in Fig.11. In Fig.11(a) and Fig. 11(c), ch1 shows the experimental waveform of the capacitor voltage, ch2 shows the experimental waveform of the DC-link voltage, ch3 shows the experimental waveform of the unfiltered ac voltage, and ch4 shows the experimental waveform of the output current. All of them are well controlled, the proposed sequential-MPC strategy does not need to adjust the weight factors, and the FFT analysis in Fig. 11(b) and Fig. 11(d) show that the THD of the output current of the traditional FCS-MPC strategy is smaller than that of sequential-MPC strategy when on steady-state. However, the difference is not big, yet the calculation is simpler, proving that the model prediction using the weight elimination technique can also basically achieve the effect of the traditional FCS-MPC.

B. Power Step-Change

Given the input voltage v_{in} = 100 V and DC-link voltage U_{dc} = 200 V, when the output power reference P_{o_ref} changes from 1000 W to 540 W, the experimental results are shown in Fig. 12. In both strategies, the capacitor voltage remains unchanged and stable at approximately 50 V, the DC-link voltage remains unchanged and is boosted to approximately 200 V, and the output current abruptly changes from 8.165 A to 6 A. It is

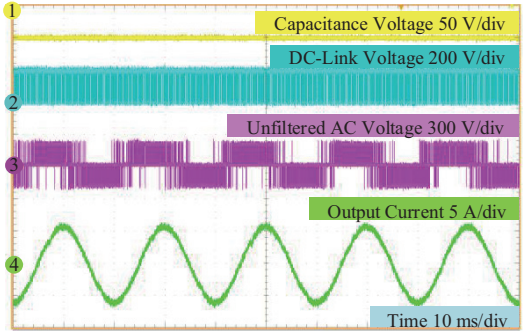

(a) Experimental waveform of steady-state in the traditional FCS-MPC strategy

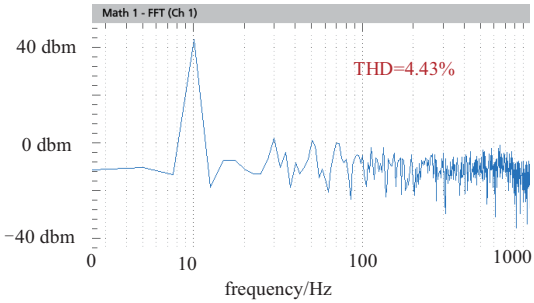

(b) Output current FFT analysis of the traditional FCS-MPC strategy

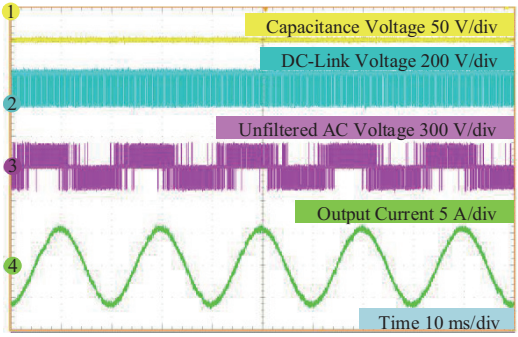

(c) Experimental waveform of steady-state in the proposed sequential-MPC strategy

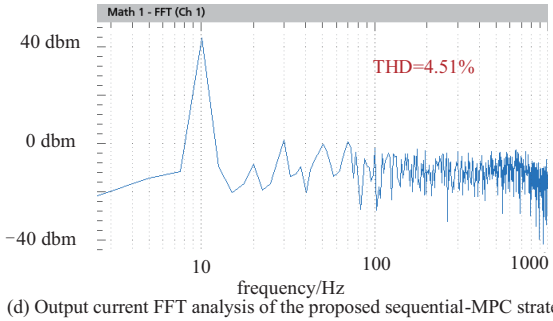

(d) Output current FFT analysis of the proposed sequential-MPC strategy

Fig. 11. Steady-state experimental waveforms.

evident that the two strategies in the output power steps state, The control quantities can track the reference value well, and the waveforms match those in the simulation analysis after the step-change in power.

C. DC-Link Voltage Step-Change

Given the input voltage v_{in}=100 V and the output power

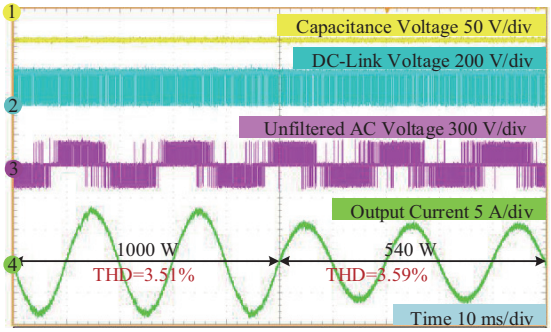

(a) Experimental waveform of load current step-change in the traditional FCS-MPC strategy

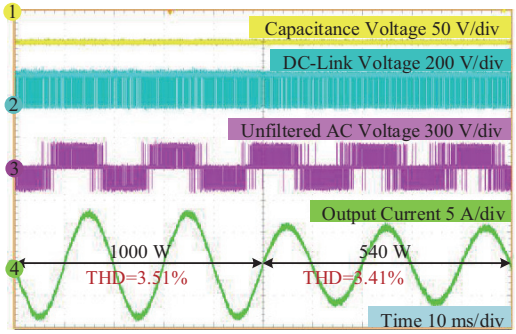

(b) Experimental waveform of load current step-change in the proposed sequential-MPC strategy

Fig. 12. Experimental results when output power reference value steps from 1000 W to 540 W.

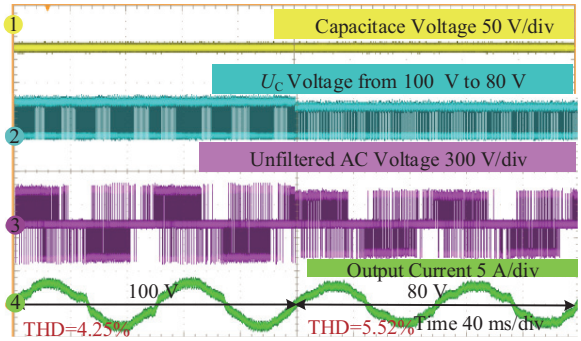

(a) Experimental waveform of a DC-link voltage reference value step-change in the traditional FCS-MPC strategy

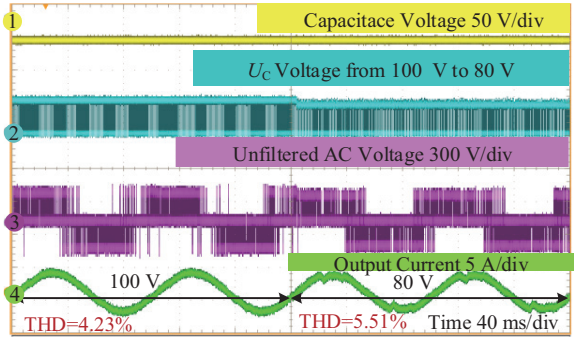

(b) Experimental waveform of DC-link voltage reference value step-change in the proposed sequential-MPC strategy

Fig. 13. Experimental waveforms when DC-link voltage reference value steps from 100 V to 80 V.

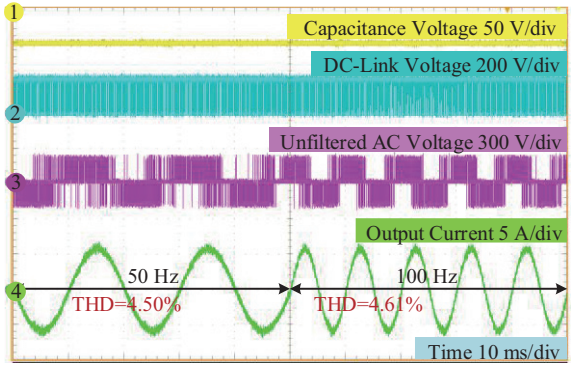

(a) Experimental waveform of output frequency reference value step-change in the traditional FCS-MPC strategy

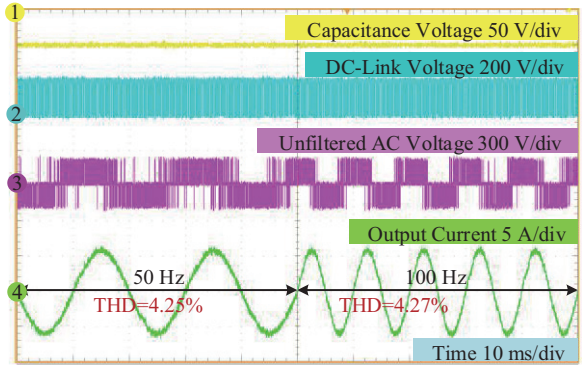

(b) Experimental waveform of output frequency reference value step-change in the proposed sequential-MPC strategy

Fig. 14. Experimental waveforms output when the output frequency reference value abruptly changes from 50 Hz to 100 Hz.

reference value P_{o_ref} = 540 W. When the DC-link voltage reference value abruptly changes from 100 V to 80 V, the experimental results are shown in Fig. 13. The capacitor voltage and the DC-link voltage can be kept stable in the traditional FCS-MPC strategy and the proposed sequential-MPC strategy. It can be seen that under this condition, the proposed sequential-MPC can also achieve similar results as the FCS-MPC strategy.

D. Frequency Step-Change

In this experiment given the input voltage v_{in} = 100 V, the DC-link voltage U_{dc}= 200 V remains unchanged, and the output power reference value P_{o_ref} = 540 W, when the output frequency reference value abruptly changes from 50 Hz to 100 Hz. The experimental results are shown in Fig. 14. In both strategies, the capacitor voltage and the DC-link voltage can follow the reference value well. Each control quantity can also track the reference value well in the frequency step-change case, which is consistent with the waveform of the simulation analysis after the sudden change in frequency. The FFT analysis shows that the quality of the output current of the proposed sequential-MPC strategy is better than that of the traditional FCS-MPC strategy, both before and after the sudden change in frequency.

VI. Conclusion

To solve the problem of FCS-MPC for O-ZSI with the transformer, this paper proposed an improved O-ZSI sequential-MPC strategy without weighting factors. The feasibility and effectiveness of the proposed strategy are verified by simulation analysis and experiment results.

1) The strategy proposed in this paper effectively solves the model predictive control with the transformer Z-source topology and can achieve closed-loop control, simple adjustment, and easy digital implementation.

2) Compared with the traditional FCS-MPC and traditional S-MPC strategy, the proposed sequential-MPC strategy in this paper can balance the weights of each control variable without adjusting the weighting factors. And it has comparable when on steady state and better dynamic properties, but makes the calculations easier.

References

[1] F. Z. Peng, "Z-source inverter," in *IEEE Transactions on Industry Applications*, vol. 39, no. 2, pp. 504–510, Mar.-Apr. 2003.

[2] M. -K. Nguyen, Y. -C. Lim, and G. -B. Cho, "Switched-inductor quasi-Z-source inverter," in *IEEE Transactions on Power Electronics*, vol. 26, no. 11, pp. 3183–3191, Nov. 2011.

[3] J. Anderson and F. Z. Peng, "Four quasi-Z-Source inverters," in *2008 IEEE Power Electronics Specialists Conference*, Rhodes, Greece, 2008, pp. 2743–2749.

[4] W. Qian, F. Z. Peng, and H. Cha, "Trans-Z-source inverters," in *IEEE Transactions on Power Electronics*, vol. 26, no. 12, pp. 3453–3463, Dec. 2011.

[5] P. C. Loh, D. Li, and F. Blaabjerg, "Γ-Z-source inverters," in *IEEE Transactions on Power Electronics*, vol. 28, no. 11, pp. 4880–4884, Nov. 2013.

[6] M. -K. Nguyen, Y. -C. Lim, and S. -J. Park, "Improved trans-Z-source inverter with continuous input current and boost inversion capability," in *IEEE Transactions on Power Electronics*, vol. 28, no. 10, pp. 4500–4510, Oct. 2013.

[7] Z. Aleem and M. Hanif, "Operational analysis of improved Γ-Z-source inverter with clamping diode and its comparative evaluation," in *IEEE Transitions on Industrial Electronics*, vol. 64, no. 12, pp. 9191–9200, Dec. 2017.

[8] A. Moghassemi, S. Padmanaban, V. K. Ramachandaramurthy, M. Mitolo, and M. Benbouzid, "A novel solar photovoltaic fed transZSI-DVR for power quality improvement of grid-connected PV systems," in *IEEE Access*, vol. 9, pp. 7263–7279, 2021.

[9] Z. Aleem and M. Hanif, "Improved Γ-Z-source inverter," in *2016 IEEE Energy Conversion Congress and Exposition (ECCE)*, Milwaukee, WI, USA, 2016, pp. 1–5.

[10] Y. Liu, H. Abu-Rub, and B. Ge, "Z-source/quasi-Z-source inverters: derived networks, modulations, controls, and emerging applications to photovoltaic conversion," in *IEEE Industrial Electronics Magazine*, vol. 8, no. 4, pp. 32–44, Dec. 2014.

[11] O. Ellabban and H. Abu-Rub, "Z-source inverter: topology improvements review," in *IEEE Industrial Electronics Magazine*, vol. 10, no. 1, pp. 6–24, Mar. 2016.

[12] S. Vazquez, J. I. Leon, L. G. Franquelo, J. Rodriguez, H. A. Young, A. Marquez, and P. Zanchetta, "Model predictive control: A review of its applications in power electronics," in *IEEE Industrial Electronics Magazine.* vol. 8, no. 1, pp. 16–31, Mar. 2014.

[13] J. Rodriguez, M. P. Kazmierkowski, J. R. Espinoza, P. Zanchetta, H. Abu-Rub, H. A. Young, and C. A. Rojas, "State of the art of finite control set model predictive control in power electronics," in *IEEE Transitions on Industrial Electronics*, vol. 9, no. 2, pp. 1003–1016, May 2013.

[14] S. Kouro, P. Cortes, R. Vargas, U. Ammann, and J. Rodriguez, "Model predictive control-a simple and powerful method to control power converters," in *IEEE Transitions on Industrial Electronics*, vol. 56, no. 6, pp. 1826–1838, Jun. 2009.

[15] A. Bakeer, M. A. Ismeil, and M. Orabi, "A powerful finite control set-model predictive control algorithm for quasi-Z-source inverter," in *IEEE Transactions on Industrial Informatics*, vol. 12, no. 4, pp. 1371–1379, Aug. 2016.

[16] M. Mosa, R. S. Balog, and H. Abu-Rub, "High-performance predictive control of quasi-impedance source inverter," in *IEEE Transactions on Power Electronics*, vol. 32, no. 4, pp. 3251–3262, Apr. 2017.

[17] Y. Liu, H. Abu-Rub, Y. Xue, and F. Tao, "A discrete-time average model-based predictive control for a quasi-Z-source inverter," in *IEEE Transactions on Industrial Electronics*, vol. 65, no. 8, pp. 6044–6054, Aug. 2018.

[18] H. M. Kojabadi, H. F. Kivi, and F. Blaabjerg, "Experimental and theoretical analysis of trans-Z-source inverters with leakage inductance effects," in *IEEE Transactions on Industrial Electronics*, vol. 65, no. 2, pp. 977–987, Feb. 2018.

[19] A. Ayad, P. Karamanakos, and R. Kennel, "Direct model predictive current control strategy of quasi-Z-source inverters," in *IEEE Transactions on Power Electronics*, vol. 32, no. 7, pp. 5786–5801, Jul. 2017.

[20] S. Sajadian and R. Ahmadi, "Model predictive control of dual-mode operations Z-source inverter: islanded and grid-connected," in *IEEE Transactions on Power Electronics,* vol. 33, no. 5, pp. 4488–4497, May 2018.

[21] X. Duan, L. Kang, H. Zhou, and Q. Liu, "Multivector model predictive power control with low computational burden for grid-tied quasi-Z-source inverter without weighting factors," in *IEEE Transactions on Power Electronics*, vol. 37, no. 10, pp. 11739–11748, Oct. 2022.

[22] Y. Xu, Y. He, and S. Li, "Logical operation-based model predictive control for quasi-Z-source inverter without weighting factor," in *IEEE Journal of Emerging and Selected Topics in Power Electronics*, vol. 9, no. 1, pp. 1039–1051, Feb. 2021.

[23] Y. Guo, H. Sun,Y. Zhang, Y. Liu, X. Li, and Y. Xue, "Duty-cycle predictive control of quasi-Z-source modular cascaded converter based photovoltaic power system," in *IEEE Access*, vol. 8, pp. 172734–172746, 2020.

[24] Y. Xu and H. Xiao, "Combinative voltage vector-based model predictive control for performance improvement of quasi Z-source inverter," in *IEEE Access*, vol. 9, pp. 143013–143025, 2021.

[25] A. Bakeer, G. Magdy, A. Chub, and D. Vinnikov, "Predictive control based on ranking multi-objective optimization approaches for a quasi-Z source inverter," in *CSEE Journal of Power and Energy Systems*, vol. 7, no. 6, pp. 1152–1160, Nov. 2021.

[26] Y. Xu, Y. He, H. Li, and H. Xiao, "Model predictive control using joint voltage vector for quasi-Z-source inverter with ability of suppressing current ripple," in *IEEE Journal of Emerging and Selected Topics in Power Electronics*, vol. 10, no. 1, pp. 1108–1124, Feb. 2022.

[27] Y. Zhang, B. Zhang, H. Yang, M. Norambuena, and J. Rodriguez, "Generalized sequential model predictive control of IM drives with field-weakening ability," in *IEEE Transactions on Power Electronics*, vol. 34, no. 9, pp. 8944–8955, Sept. 2019.

[28] S. A. Davari, D. A. Khaburi, and R. Kennel, "An improved FCS–MPC algorithm for an induction motor with an imposed optimized weighting factor," in *IEEE Transactions on Power Electronics*, vol. 27, no. 3, pp. 1540–1551, Mar. 2012.

[29] T. Geyer, "Algebraic weighting factor selection for predictive torque and flux control," in *Proceedings of 2017 IEEE Energy Conversion Congress and Exposition* (*ECCE*), Cincinnati, OH, USA, 2017, pp. 357–364.

[30] C. A. Rojas, J. Rodriguez, F. Villarroel, J. R. Espinoza, C. A. Silva, and M. Trincado, "Predictive torque and flux control without weighting factors," in *IEEE Transactions on Industrial Electronics*, vol. 60, no. 2, pp. 681–690, Feb. 2013.

[31] M. Norambuena, J. Rodriguez, Z. Zhang, F. Wang, C. Garcia, and R. Kennel, "A very simple strategy for high-quality performance of AC machines using model predictive control," in *IEEE Transactions on*

Power Electronics, vol. 34, no. 1, pp. 794–800, Jan. 2019.

[32] J. Rodas, O. Gonzalez, M. Norambuena, J. Doval-Gandoy, O. Gomis-Bellmunt, R. Gregor, M. Ayala, J. Rodríguez, and C. Romero, "Weighting-factorless sequential model predictive torque control of a six-phase AC machine," in *Proceedings of 2023 IEEE Conference on Power Electronics and Renewable Energy* (*CPERE*), Luxor, Egypt, 2023, pp. 1–5.

[33] J. Zhang, L. Li, M. Norambuena, J. Rodriguez, and D. G. Dorrell, "Sequential model predictive control of direct matrix converter without weighting factors," in *IECON 2018 - 44th Annual Conference of the IEEE Industrial Electronics Society*, Washington, DC, USA, 2018, pp. 1477–1482.

[34] M. Aly, F. Carnielutti, A. Shawky, E. M. Ahmed, M. Norambuena, S. Kouro, and J. Rodriguez, "Weighting factorless sequential model predictive control method with fixed switching frequency for five-level T-type photovoltaic inverters," in *IECON 2021-47th Annual Conference of the IEEE Industrial Electronics Society*, Toronto, ON, Canada, 2021, pp. 1–6.

Xuan Wang was born in Shandong, China, in 1997. She received the B.S. degree in Electronic Information Engineering from Shanghai University of Technology, China, in 2020. She is currently pursuing the Master degree in electric engineering with University of Shanghai for Science and Technology, Shanghai, China. Her current research interests include Z-source inverter.

Wei Luo was born in Shanxi, China, in 1986. He received the B.S. degree in electrical engineering and automation from the China University of Mining and Technology, Xuzhou, China, in 2009, M.S. and Ph.D. degrees in electric engineering from Shanghai Jiao Tong University, Shanghai, China, in 2012 and 2018.

He is currently an Associate Professor of electrical engineering with University of Shanghai for Science and Technology, China. His research interests include multilevel converters, high-power motor drives, and internet of things.